Maximal interferon induction by influenza lacking NS1 is infrequent owing to requirements for replication and export

Alison C. Vicary[1], Asama Lekbua[1], Jack Reddan[1], Zaida K. Rodriguez[1], Marisa Mendes[1], Alistair B. Russell[1*],

1 School of Biological Sciences, University of California, San Diego, La Jolla, CA, United States of America

¤School of Biological Sciences, University of California, San Diego, La Jolla, CA, United States of America
* a5russell@ucsd.edu

Abstract

Influenza A virus exhibits high rates of replicative failure due to a variety of genetic defects. As such, most viral particles cannot complete the life cycle. However, despite this failure, this virus is incredibly successful in the suppression of innate immune detection and the production of interferons, succeeding at remaining undetected in >99% of cells in tissue-culture models of infection. As the same variation that leads to replication failure can, by chance, inactivate the major innate immune antagonist in influenza A virus, NS1, what features prevent these events from triggering massive amounts of interferon production? By studying how genetic and phenotypic variation in a viral population lacking NS1 correlates with interferon production, we have built a model of the "worst-case" failure from an improved understanding of the steps at which NS1 acts in the viral life cycle to prevent triggering of an innate immune response. In doing so, we find that NS1 prevents the detection of *de novo* innate immune ligands, defective viral genomes, and viral export from the nucleus. Taken together, the highest level of stimulation we observe (97% of infected cells), requires a high level of replication in the presence of defective viral genomes with NS1 and NS1 alone from the NS segment bearing an inactivating mutation. This is incredibly unlikely to occur within the standard variation found within a viral population, and would generally require direct, artificial, intervention to achieve at an appreciable rate. Thus from our study, we procure at least a partial explanation for the seeming contradiction between high rates of replicative failure and the rarity of the interferon response to influenza infection.

Author summary

The production of interferons in response to viral threat is a potent barrier to successful infection. Viruses like influenza A virus encode potent interferon antagonists, suppressing detection of viral replication such that only an incredibly rare minority of cells successfully produce interferons. Curiously, even in the absence of its major interferon antagonist, NS1, influenza only induces an interferon response in a minority of infected cells. Using a combination of single-cell RNAseq, flow cytometry, and classical bulk methods, we explored how heterogeneity, both genetic and phenotypic, in a virus lacking NS1, explains the observed rarity of the interferon response. In doing so, we find that, in the absence of NS1, viral replication is absolutely required to induce an

interferon response, and that both active export and the presence of defective viral genomes greatly enhance the detection of this virus. The confluence of events which we find maximizes the host response is incredibly unlikely to occur alongside the absence of the NS1 protein via the most common forms of genetic variation in the viral population, perhaps explaining, in part, how a virus with such a high error rate nevertheless has such a high rate of success at evading cell intrinsic innate immunity.

Introduction

Nearly every cell in the human body is capable of detecting viral infection and responding via the production of type I and, for mucosal cells, type III interferons. [1] These signaling proteins, in turn, alert neighboring cells to a pathogenic threat and stimulate the production of hundreds of interferon-stimulated genes, including both restriction factors, which prevent viral entry and growth, as well as signaling proteins that recruit additional components of the mammalian immune system. [2] The production of interferons by infected epithelial cells and the subsequent antiviral response presents a considerable barrier to successful viral infection. Treatment with interferons, or with ligands or mutant viruses primed to induce interferons, prior to infection is strongly protective. [3, 4]

As a testament to its importance, every successful viral pathogen of humans antagonizes, evades, or otherwise subverts interferon production in infected cells. [5] Influenza A virus, a segmented, negative-sense RNA virus, and the predominant causative agent of human flu, is no exception. This virus engages in several strategies that allow it to evade the induction of interferons with a high degree of success. Chief among these is the production of nonstructural protein 1 (NS1), a multifunctional protein that, among other activities, antagonizes RIG-I, a major sensor of influenza A virus replication products. [6] In a 1998 study by García-Sastre et al., it was found that inactivating mutations in the NS1 gene, which is not essential, resulted in a massive increase in the production of interferons in response to this virus. [7] However, even in the absence of this, important, immune antagonist, influenza A virus still only evokes a response in a fraction of infected cells. [8] This suggests that additional viral strategies antagonizing interferons, or, alternatively, standing variation in the viral-cycle, may drive incomplete detection of this virus.

Redundant pathways, at least at the level of viral consensus sequence, in interferon suppression by influenza A virus are of considerable interest, as they may underlie the success of this human pathogen. As a result of a multifaceted strategy to interferon suppression, this virus, which, owing to a variety of genetic defects can only complete the viral life cycle in, at most, 10% of virions in single-particle initiated infections, nevertheless maintains interferon suppression in 99.5% of infected cells. [9–13] Why exhibit such stringent control with redundancies that overcome standing viral variation? The answer may lie in how critical even those rare cells are to the resolution of disease. Individuals with various defects in interferon pathways who lack even these rare cells have been observed to experience significantly more severe outcomes in influenza infection, and, even in the mouse model of infection, dramatic differences in outcome can be ascribed to the presence or absence of a single interferon-stimulated gene, *Mx1*. [14–16] Thus, despite their rarity, these cells have an out-sized impact on the control and resolution of disease— as interferons are diffusible, a single producing cell may impact many, many, others. We may therefore speculate that even small changes in the percentage of responding cells could have a dramatic impact on the success of a viral pathogen, thus necessitating a tight control over host detection despite considerable variation within a viral population.

To procure a deeper understanding of the relationship between influenza variation

and interferon production we measured what genetic and phenotypic features of influenza A virus correlate with interferon production in a virus lacking NS1. By ablating the function of NS1, we could concurrently study at what stages of the viral life cycle this protein provides protection, as well as, in its absence, what additional features may control the host response to this virus. In doing so we find that *de novo* viral RNA synthesis is absolutely required for interferon induction by a virus lacking the NS1 antagonist, and that induction is increased in the presence of active viral genome export. The dual requirement for replication and export, and the role of potent innate ligands such as defective viral genomes, to achieve the highest level of interferon induction in the absence of NS1 actually means the most stimulatory outcomes would be quite difficult to achieve via natural variation alone. This provides a partial explanation for how a viral population with such a high rate of mutation is, nevertheless, rarely detected by cell intrinsic innate immunity.

Results

Single cell analysis of virus lacking NS1 reveals perturbations to the viral life cycle

The NS1 protein is co-encoded in the non-structural (NS) segment with nuclear export protein (NEP), responsible for nuclear export of viral genomes in complex with ribonucleoproteins (vRNP) and the modulation of viral polymerase activity. [17–20] Transcripts produced from this segment either encode NS1 or NEP, determined by splicing at an inefficient splice site after the tenth codon of NS1 (Fig1A). In order to study the impact of inactivating NS1 alone, four in-frame stop codons were introduced downstream of the NEP splice donor in the NS segment from A/WSN/1933. This mutation, as with others that ablate NS1 function, results in a viable viral population.

In order to identify what variation in viral infection may govern the probability of a host response in the absence of the NS1 antagonist, we infected A549 cells, a human lung epithelial carcinoma cell line commonly used for influenza research, with virus bearing our mutant NS1 ($NS1_{stop}$) at an MOI of 0.2, and performed single cell RNAseq at 10h post-infection using the 10x chromium platform, which, owing to polyA tails and 5' caps present on viral mRNAS, can capture both viral and host transcripts in a single experiment. [21–24]

To correct for extracellular RNA contamination, which complicates the identification of yes/no events such as viral infection and interferon production, we included uninfected canine (MDCK-SIAT1) cells in our 10x genomics run, spiked in at a relatively low fraction of the entire population (∼5%). Human or viral RNA associated with canine cells is either due to a human cell co-occupying an emulsion (a doublet), or due to extracellular contamination (S1 Fig). We can therefore estimate both our co-occupancy rate (4.9%) where transcriptomes are, in actuality, derived from multiple cells, as well as the probability that the observed amount of any given mRNA is explainable by extracellular contamination alone. [10] From this dataset, we identify cells that are positive for influenza or type I or type III interferons based on their levels of expression in comparison to our contamination control.

Before proceeding, we wished to understand whether we should study type I and type III interferon production as a single, unified, phenomenon, or whether we should study each independently. In previous analyses using single-cell RNAseq on wild-type virus, and in flow cytometry, and in *in vivo* mouse datasets, transcription of both families of interferons during infection was found to be highly correlated. [10, 25] Therefore we tested whether the transcription of type I and type III intererons was likewise correlated in our dataset. In doing so, we find nearly all type I interferon

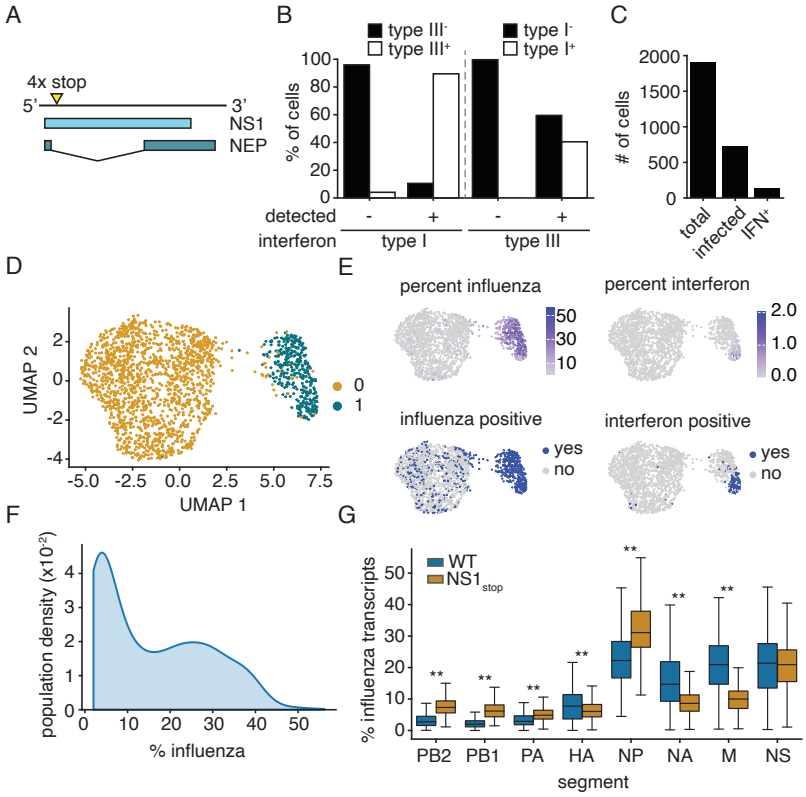

Fig 1. Single cell transcriptional analysis of A549 cells infected with $NS1_{stop}$.

(A) Diagram of the NS segment in the (+) orientation showing NS1 and NEP open-reading frames. Stop codons were introduced at the indicated site to generate $NS1_{stop}$. Full genome sequence in S1 File. **(B)** Fraction of cells annotated as positive for either type I (left) or type III (right) interferon expression were further assessed for expression of type III (left) or type I (right) interferon expression. Type I and type III expression were associated at levels unlikely to be driven by chance (Fisher's exact test $p = 3 \times 10^{-58}$) **(C)** Numbers of cells meeting indicated thresholds in our $NS1_{stop}$ single-cell RNAseq data. Analysis used to set thresholds shown in S1 Fig. **(D)** UMAP clustering of single cell transcriptomes. **(E)** Coloring of figure in **D** by percentage of transcriptome derived from influenza or interferon transcripts (top) or by our positivity calls as indicated in **C** (bottom). **(F)** Distribution of the fraction of reads derived from influenza in $NS1_{stop}$ infected cells. **(G)** Fraction of influenza reads derived from the indicated segments in cells infected with either $NS1_{stop}$ or wild-type virus. Asterisks mark significantly different fractions of influenza transcripts, two-tailed t test, Benjamini-Hochberg multiple testing correction at an FDR of 0.05. Analysis used to threshold wild-type virus shown in S2 Fig

expressing cells are also positive for type III interferon expression, and the expression of type III interferons was highly correlated with positivity for type I interferons ($p = 3 \times 10^{-58}$, Fig1B). Therefore we considered production of either type I or type III (or both) interferon transcripts as "interferon positive" in our subsequent analyses. Having made this decision, we found that, of the 1901 human cells that met our thresholds for inclusion, 716 were positive for influenza, and 132 were positive for either type I or type III interferon expression (IFN) (Fig1C).

Clustering our transcriptomes by unsupervised dimensionality reduction using UMAP, we find cellular transcriptomes separate largely into two different clusters (Fig1D). We would anticipate both infection, and innate immune induction, to have dramatic impacts on the transcriptome. Consistent with our expectations, the frequency of viral transcripts distributes between these two UMAP clusters, and the percentage of type I or type III interferon transcripts likewise defines a locally-clustered group within a larger UMAP grouping. Our binary, influenza positive, and interferon positive, calls, map similarly (Fig1E).

Within those cells we identify as infected by influenza, as with prior studies on wild-type virus, we see a wide dispersion of influenza transcript frequencies, indicating the durability of this phenomenon to the presence or absence of NS1 (Fig1F). [10,26,27] Additionally, as with wild-type virus, we see that, generally, despite this variation, each segment contributes a relatively consistent frequency of transcripts to the overall pool of influenza mRNAs (Fig1G). Here we collapse the two segments that generate spliced mRNAs, matrix (M) and NS, into single measurements each rather than as M1, M2, NS1, and NEP, as the 3' sequencing method employed in the 10x Chromium workflow incompletely captures the splice junction of these transcripts, complicating their measurements.

Despite the relative consistencies of the frequencies observed in the $NS1_{stop}$ variant, we find that they deviate considerably from those observed in wild-type A/WSN/1933. Comparing to a contemporaneously-generated wild-type control (S2 Fig), there is a significant difference in the fraction of influenza transcripts derived from each segment save for, curiously, NS itself (Fig1G). This difference is most apparent in the greatly diminished frequency of transcripts derived from the M and neuraminidase (NA) segments, and a concordant increase in the relative frequency of transcripts derived from the segment encoding nucleoprotein (NP).

Interferon induction by $NS1_{stop}$ associated with active influenza transcription

Prior to exploring the contribution of viral variation to the observed response to $NS1_{stop}$, we wished to assess the degree to which interferon induction is associated with infection. While, in general, it is thought that RIG-I-dependent interferon production during influenza infection is restricted to those cells in which the virus has successfully delivered its genomic material, a recent tissue-culture study suggested a role for bystander cells. [28] As variation in uninfected cells would be host-derived, we wished to first establish whether measuring interferon production strictly in light of direct viral infection was warranted in the context of an $NS1_{stop}$ virus.

Comparing production of interferons in influenza-infected cells to those that fail to meet our thresholds for inclusion, we find a strong statistical association between infection and the production of interferons ($p = 1.7 \times 10^{-48}$, Fig2A). While ∼16% of infected cells are producing interferons, only ∼0.6% of cells that fail to meet our thresholds for influenza positivity were found to be positive for interferon induction. To confirm this finding, we use a previously-validated interferon-reporter A549 cell line that expresses eGFP downstream of the IL29 (interferon lambda-1, IFNL1) promoter. [10]

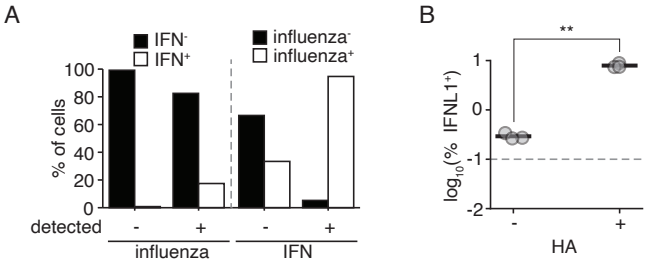

Fig 2. Interferon induction is associated with active viral transcription in an $NS1_{stop}$ infection.
(A) Fraction of cells in our single-cell transcriptomic dataset annotated as positive for either influenza infection (left) or interferon expression (right) were further assessed for expression of interferon (left) or influenza infection (right). Influenza infection and interferon were associated at levels unlikely to be driven by chance (Fisher's exact test, p=4.5 x 10^{-47}) **(B)** A549 IFNL1 reporter cells were infected with $NS1_{stop}$ at an MOI of 0.1, fixed, and stained for the viral HA 13h post infection, and analyzed by flow cytometry. The fraction of cells staining positive for HA exhibits a significantly higher probability of IFNL1 reporter expression, two-tailed t test, p=0.003. The dotted line indicates the detection limit as set on an uninfected control. Individual replicates shown, n=3. Full staining and gates in S3 Fig.

Infecting this cell line at an MOI of 0.1, and staining for the viral protein hemagglutinin (HA), we find that rates of interferon production are close to 15-fold higher in cells we positively identify as infected. The remaining levels of interferon production in HA^- cells (∼0.4%) are above our uninfected control threshold (0.1%), and could either represent rare, paracrine, induction of interferons, or, more likely, infections that fail to produce sufficient HA to meet our thresholds (Fig2B). Overall we find that interferon production in the absence of infection is not occurring at an appreciable rate in our system, similar to previous findings using wild-type virus. [10, 25, 26]

NS1 protects against the detection of replication

We next looked for potential explanations of why only a subset of infected cells produce interferons. As viral genomes themselves, and/or products of genome replication, are anticipated to be the major ligands for innate immune sensing of influenza A virus, we looked as to whether replication could be correlated with the probability of interferon production. [29–32] While our single-cell dataset samples mRNA alone, mRNA and replication are coupled in influenza, with progeny genomes serving as templates for mRNA production later in infection. [33, 34] With that in mind, we measured whether levels of influenza transcripts were different between cells positively identified as producing interferon versus infected cells in which interferon was not detected in our single-cell dataset.

When we compare these two populations, we find that, among influenza-positive cells, those producing interferons generally had much higher levels of influenza transcription (Fig3A). This matches a prior observation that, in wild-type influenza, in infections wherein the NS segment was absent, a phenomenon observed ∼15% of the time for any given segment, interferon production was associated with higher levels of influenza transcripts. [10, 12] In this prior report, using $NS1_{stop}$, it was also found that higher levels of HA staining correlated with an increased probability of interferon induction. We recapitulate these findings, demonstrating that HA^+ $IFNL1^+$ reporter

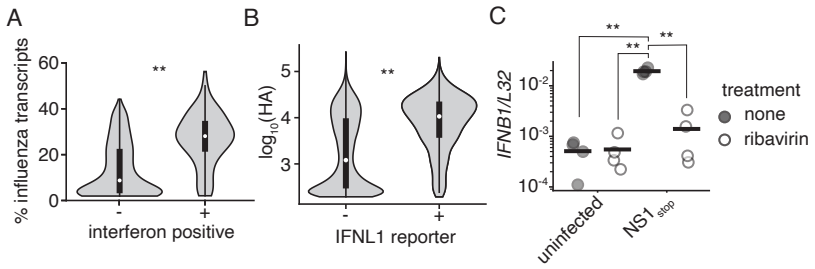

Fig 3. Detection of $NS1_{stop}$ requires active genome replication.
(A) Percentage of transcripts derived from influenza virus in our single-cell dataset in influneza$^+$ cells that were, or were not, identified to be expressing type I and III interferons. A higher level of influenza transcripts was found to be associated with interferon induction, two-tailed t test, $p = 8.8 \times 10^{-25}$ **(B)** Infection from Fig2B showing the level of HA staining in HA$^+$ cells, compared between IFNL1$^+$ and IFNL1$^-$ reporter cells, was found to be significantly different, two-tailed t test, $p < 10^{-5}$ **(C)** Cells infected, or not, with $NS1_{stop}$ were treated two hours prior to infection, or not, with 200μM ribavirin. 8 hours post-infection, *IFNB1* transcript levels were measured relative to a housekeeping control (*L32*). Asterisks indicate significant differences, ANOVA $p<0.05$, post hoc Tukey's test, $q<0.05$. n=4. Effect of ribavirin on viral replication and transcription was confirmed by concurrent qPCR against viral HA transcripts, S5 Fig.

cells stain more strongly for HA than HA$^+$ IFNL1$^-$ (Fig3B). Examing the entire breadth of HA staining, we find additional statistical support for a positive correlation between HA staining and the probability that any given cell is IFNL1$^+$ (S4 Fig).

While it would seem unlikely that high levels of transcription are the result of interferon production, our results do not establish whether these events are causal or correlated, nor, if causal, the direction of causality. We turn to an inhibitor we have used to study this phenomenon previously, ribavirin. [35] Ribavirin is a nucleoside analog, and at high concentrations can inhibit the viral polymerase. [36, 37] When treated with ribavirin, interferon transcription in response to $NS1_{stop}$ is suppressed to uninfected levels, which represent the limit of detection in our qPCR (Fig3C). Thus not only is the probability of interferon induction impacted by the level of viral replication for $NS1_{stop}$, but, NS1 appears to be solely responsible for preventing the detection of *de novo* generated innate immune ligands. Other mechanisms, such as occlusion of triphosphate vRNA ends by the viral polymerase, may be responsible for masking RIG-I ligands upon entry into the cell during transit to the nucleus. This is consistent with our overall understanding of NS1, which is at most, only present in viral particles at an incredibly low concentration, and thus likely cannot impact interferon production until it has reached higher levels later in infection. [38]

Defective particles variously impact interferon induction in the absence of NS1

Defective influenza A virus genomes, generally bearing large internal deletions in the three segments encoding the viral polymerase, are associated with interferon induction. [27, 32, 35, 39] We therefore investigated whether large internal deletions contribute to the variable detection of $NS1_{stop}$ virus. While the 3' sequencing we used in our workflow incompletely samples viral genotypes, we could, still identify infections in which deletions were present, and measure whether they co-associate with the production of interferons at a rate greater than expected by chance. Setting empirical thresholds based on an inflection curve of deletion abundance (S6 Fig), we find a

spectrum of deletions that we may confidently associate with individual infections in our dataset. Curiously, this set is not as enriched in polymerase deletions as we would expect from other, bulk, sequencing, still, the most common segment bearing a deletion remains a polymerase segment, PB1 (Fig4A).

Deletions were a rare occurrence in this dataset, identified in only 6.8% of infections (Fig4B). While rare, they do associate with interferon production at an increased, statistically significant, rate (Fig4C). However, confounding this measurement, our ability to successfully identify a deletion would be expected to be correlated with the number of transcripts recovered from a given infection, particularly for a 3' sequencing approach. Consistent with this concern, observation of a deletion was associated with higher levels of influenza transcripts (Fig4D). This is curious, as, in general, deletions would be expected to impede genome replication. Explaining this discrepancy, all deletions identified were present in a mixture with predicted full-length transcripts, either due to coinfection or *de novo* generation during replication (Fig4E). When we only consider high transcription infections (those that match the median transcript levels associated with deletions) we still see an association between interferon and deletions, but this relationship is considerably weaker and is not statistically significant (Fig4F). Nevertheless, we know from our prior work that not all deletions associate with interferon induction, and thus our weak association found here did motivate us to probe further using populations with deliberate differences in defective virus burden. [35]

We therefore generated WT and $NS1_{stop}$ populations with differing compositions of defective particles. Defective particles can accumulate in high abundance in a viral population when grown at a high MOI, as coinfection and complementation allow the propagation of these otherwise replication-incompetent viruses. [40] By passaging virus at high MOI, we were able to generate viral populations with a high burden of defective particles, which we validated possessed an increased genome to infectivity ratio relative to a "low-defective virus" control (Fig5A).

We might expect defective viral particles to play a complex, dose-dependent role in the interferon response to $NS1_{stop}$. While they may, in-and-of-themselves enhance detection of viral infection, at a low MOI, in the absence of coinfection, they should also produce infections that generally lack the ability to perform genome replication owing to absence of full-length polymerase. As replication is necessary in order for $NS1_{stop}$ to be detected by the host at appreciable levels, do defective particles enhance, or suppress, the immune stimulation by a virus lacking NS1? We investigated this question in both low and high MOI infections—in the former, we expect little to no complementation and thus suppression of replication, and in the latter, complementation and genome replication. Using an equivalent number of total viral particles, we infected our IFNL1 reporter cells with either low- or high-defective $NS1_{stop}$ viral populations at an MOI of either 0.1 or 5. We included a wild-type high and low-defective control, to compare the impacts of defective viral particles alone versus in the context of an $NS1_{stop}$ mutation.

Repeating prior observations, we see that high abundance of defectives in a wild-type virus background has little impact on interferon induction at low MOI but leads to a large increase in the percentage of interferon-expressing cells in higher MOI infections (Fig5B). Notably, for these measurements we take the interferon-positive fraction of all cells, rather than of the infected cells, as the lower transcription in defective particles can make flu proteins difficult to detect by flow cytometry, limiting the ability to accurately identify cells as flu-positive or flu-negative.

As expected, all $NS1_{stop}$ populations exhibited increased interferon induction relative to wild-type virus under all conditions, but the effect of defective particles varied depending on MOI (Fig5B). At a particle-corrected MOI of 0.1, $\sim$2.7% of cells were positive for the IFNL1 reporter after infection with the low-defective $NS1_{stop}$. This decreased to $\sim$0.7% for the high-defective $NS1_{stop}$ population. Thus when coinfection is

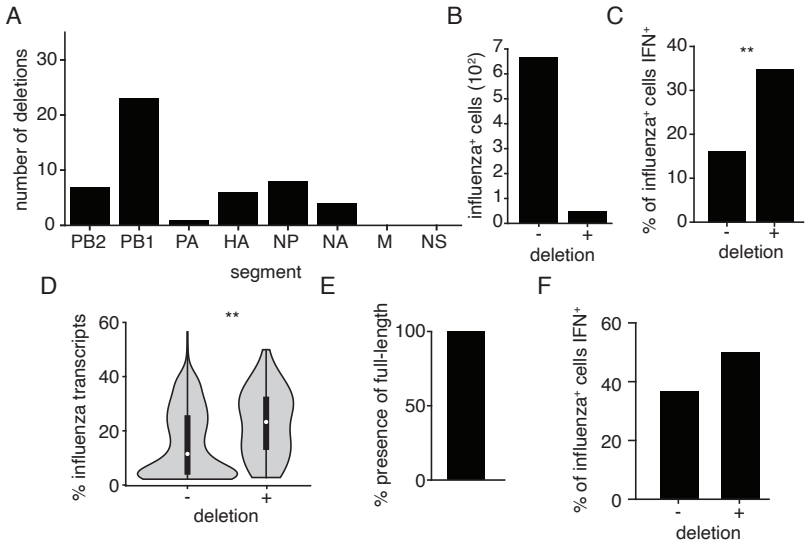

Fig 4. Deletions associate weakly with interferon induction in our $NS1_{stop}$ single-cell dataset.
(A) Number of unique cell/deletion combinations observed for each segment in our single-cell transcriptomics dataset. **(B)** Number of cells called as infected with, or without, a detectible deletion. **(C)** Fraction of cells with, and without, detectible deletions identified as interferon-positive. Asterisk indicates significant difference, Fisher's exact test p=0.002. **(D)** Percentage of transcripts derived from influenza in infected cells in which deletions were, and were not, identified. Asterisk indicates significant difference, two-tailed t test, p=0.0002. **(E)** Percentage of infections in which deletions were identified that also had junction-excluding reads (likely indicating the presence of full-length segment) at a fraction meeting our thresholds for individual segment expression. **(F)** Fraction of cells with, and without, detectible deletions identified as interferon-positive, considering only infections with a greater fraction of influenza transcripts than the median value observed in infections in which deletions were confidently identified. Populations were not found to be significantly different by Fisher's exact test (p=0.27).

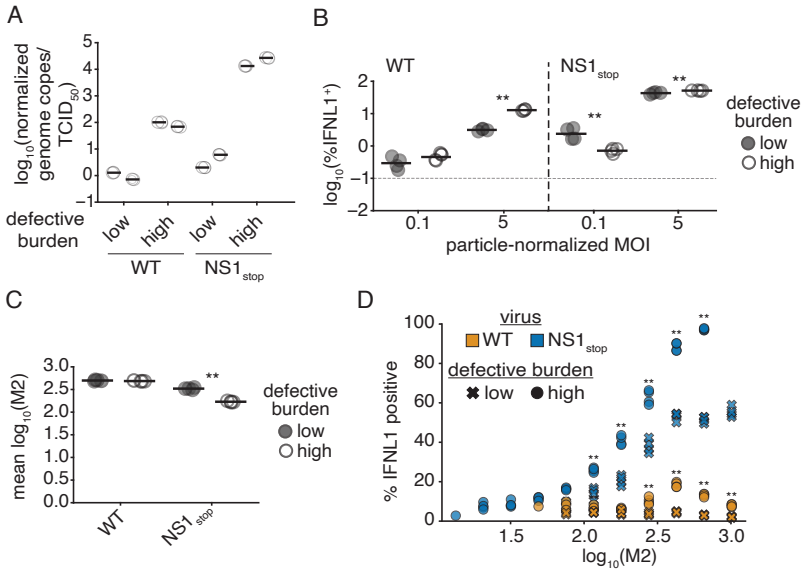

Fig 5. Defective particles can enhance, or suppress, interferon induction by $NS1_{stop}$ depending on the MOI and replication efficiency.
(A) Normalized genome copies to infectivity ratio in indicated populations. Genome copies were measured by triplicate qPCR measurements of the PA segment. Infectivity was measured by tissue-culture infectious dose 50 ($TCID_{50}$). The average ratio of these values was set to 1 for our wild type low-defective population, and then all values were calculated relative to that reference. High defective burden populations confirmed to have a greater genome/copy to infectivity ratio. Individual points indicate technical replicates, sets of three points under the same heading represent biological duplicate populations. **(B)** Percentage of total cells expressing interferon when IFNL1-reporter cells are infected with the indicated populations at the indicated particle-corrected MOI. MOI was calculated on low-defective populations, then an identical number of genome copies were added as measured in **A**. Asterisks denote significant differences between high- and low-defective populations, two-tailed t test with Benjamini-Hochberg multiple testing correction at an FDR of 0.05, n=4, two replicates of each of the biological replicate populations shown in **A. Full flow data shown in S7 Fig. (C) Mean fluorescence intensity of M2 staining in the indicated populations when added at a particle-corrected MOI of 5. Asterisks denote significant differences between high- and low-defective populations, two-tailed t test with Benjamini-Hochberg multiple testing correction at an FDR of 0.05, n=4. Full distributions shown in S8 Fig. (D) Interferon positivity in MOI 5 infections from B, divided into bins of M2 expression. Asterisks indicate significant differences between high- and low-defective populations within a viral variant. Two-tailed t test with Benjamini-Hochberg multiple testing correction at an FDR of 0.05, n=4. Statistics only calculated for M2 bins wherein all replicates across both high- and low-defective populations had greater than 100 events measured. When less than 100 events were measured, individual datapoints were excluded from the graph.**

rare, defective particles appear to dampen interferon induction associated with the loss of NS1. In contrast, at an MOI of 5, when >95% of cells should be experiencing infection from multiple viral particles, defectives are associated with a significant increase in the fraction of interferon expressing cells in a $NS1_{stop}$ background. The observation that defective particles can have opposing effects on interferon induction by $NS1_{stop}$ depending on the MOI suggests that the presence of defective genome segments can enhance the interferon response to $NS1_{stop}$ virus, but only when *de novo* replication products are generated, otherwise they are suppressive.

Still, even in the high MOI $NS1_{stop}$ infections, the enhancement in the interferon response associated with defective viral particles was relatively small, increasing the percentage of IFNL1-positive cells from ∼45% to ∼55%—similar to the relatively small difference we measured in our single-cell dataset (Figs4F, 5B). We wondered what was underlying this mild impact, for instance, is 55% perhaps the maximum achievable response? In addition to measuring the interferon response with our reporter, we concurrently stained infections shown in Fig5B for the viral protein M2. Examining M2 staining as a proxy for viral transcription, in turn a proxy for replication, we find that, in our high-defective $NS1_{stop}$ population that M2 staining is reduced (Fig5C). While this is not observed in our wild-type infections, we do note that, despite being propagated under equivalent conditions, our high-defective $NS1_{stop}$ accumulated several orders of magnitude more replication-incompetent particles. It is unclear whether this is due to differences in growth kinetics, or is a phenomenon unique to NS1. With such a high enrichment of defective particles, many coinfections may struggle to produce sufficient polymerase to support robust replication.

To measure whether, in those infections in which replication is supported, more extreme differences can be observed, we divided each infection in our high MOI regime into bins of M2 expression and assessed the fraction of cells producing interferon in each bin (Fig5D). Strikingly, not only does our high-defective $NS1_{stop}$ population exhibit increased interferon induction within each expression bin, but, at the highest levels of expression, this population triggers the production of interferons in an astounding ∼97% of cells! Conversely, a population lacking NS1, but also with a low level of defective particles, appears to saturate at ∼53% of cells responding. When we compare the M2 bin of greatest response in a wild-type high defective population, ∼20%, we would anticipate if these two interferon-stimulatory events (deletions and absence of NS1) were wholly independent, that the response would be ∼62%, much lower than ∼97%. Therefore, under conditions supporting high-levels of *de novo* synthesis of viral replication products, NS1 helps to suppress the detection of defective species, as its absence, and the presence of defective particles, are synergistic.

Segment absence partitions non-randomly with interferon induction

While the relative expression of each segment to one-another is relatively tight, segments can be stochastically lost from an infection. [12] We therefore compared the percentage of each segment that failed to meet our detection threshold between cells wherein we detect interferon and those in which we do not in our single-cell dataset (Fig6A, top). We observe that segment presence, as a general phenomenon, is associated with interferon production, meeting statistical significance for all three polymerase segments, HA, NA, and M. The former is consistent with our findings that NS1 protects against the detection of *de novo* generated innate immune ligands. However, as far as the other segments, we initially had no clear hypothesis. However, high levels of flu transcription are also consistent with an increased probability of coinfection, which suppresses segment absence, and so it is possible that what we see is driven by this correlation.

To address that possibility, we analyzed only those infections with transcript levels higher than the median observed in our interferon positive population (Fig6A, bottom). Under this new regime, we never observe the absence of any of the polymerase segments, nor nucleoprotein, all required for genome replication. For the remaining segments, unfortunately, we do not see statistically significant differences, although in part this is likely due to the relatively small number of events; a set of only 63 interferon positive cells, and 93 counterparts. Regardless, using these data to generate a hypothesis rather than demonstrate some ground truth, we still see a relatively large, if not statistically significant after multiple-hypothesis correction, difference in the M segment, as well as a two-fold association of absence with reduced interferon production for the NS segment.

To determine whether these differences were repeatable with an increased number of cells, we used flow cytometry to measure the presence of the NS segment, using an antibody against NS1 that retains staining even in our $NS1_{stop}$ mutant, and the presence of the M segment, using an antibody against M2, in an $NS1_{stop}$ infection of IFNL1 reporter cells (S10 Fig). To minimize bias caused by instances of low flu expression being falsely identified as segment absence due to staining inefficiency, we only looked at cells with high M levels, as defined by staining above the median M level observed in interferon-positive cells. Among these M-high cells, we see that cells positive for the NS segment were more likely to express interferon compared to cells lacking the NS segment (Fig6B). Similarly, when we gate on cells with high NS expression and examine the impact of M segment presence, we see that M-positive cells were also more likely to express interferon compared to cells lacking expression from the M segment. These phenotypes may even be more extreme across the whole population, as we are limited to only considering relatively high levels of influenza replication to be certain of our staining thresholds. As a control, we stained infected cells for NS and HA, and among NS-high cells, we do not see any association of HA with interferon expression. These results suggest that in $NS1_{stop}$ infection, loss of either the NS or M segment is associated with a decrease in interferon induction.

Nuclear export is required for maximal interferon induction by $NS1_{stop}$

As $NS1_{stop}$ lacks a functional NS1, the association of the NS segment with interferon indicates that the function of NEP, the other influenza A protein co-encoded with NS1 on the NS segment, is contributing to interferon induction. This is especially interesting given the role of NEP in influenza genome export. After influenza genome segments are replicated in the nucleus, NEP forms part of a binding complex that facilitates export of the newly synthesized vRNPs to the cytoplasm so that they may be packaged into new viral particles. [19] In addition to NEP, nuclear export of vRNPs involves the influenza protein M1, which is encoded on the M segment, as well as the human nuclear export factor CRM1. [41–44] Given that interferon induction by $NS1_{stop}$ virus is dependent on genome replication, nuclear export may also be critical to interferon induction, as it would expose the *de novo* influenza replication products to cytoplasmic nucleic acid sensors such as RIG-I. We hypothesized that the loss of NEP or M1 due to loss of the NS or M genome segments, respectively, decreases interferon induction in the $NS1_{stop}$ virus due to decreased nuclear export of vRNPs.

To test whether the process of vRNP nuclear export contributes to interferon induction by $NS1_{stop}$ virus, we treated infected cells 3 hours post infection with the CRM1 inhibitor B (LMB), blocking transport of influenza genomes from the nucleus, and analyzed interferon transcript expression by qPCR 8 hours post infection (Fig7A). This treatment resulted in a ∼4.5-fold decrease in *IFNB1* transcripts as measured by qPCR. The impact of LMB on influenza replication appeared modest and not

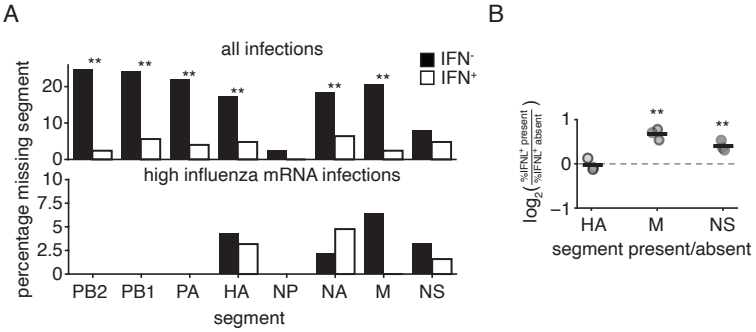

Fig 6. The M and NS segment are required for maximal induction of interferon by $NS1_{stop}$.

(A) (top)Frequencies at which mRNAs from a given segment fail to meet our thresholds, as defined in S10 Fig in cells identified as infected, grouped by interferon expression. (bottom) As in top, but restricted to infections with greater than the median fraction of transcripts in influenza infections identified as expressing interferon. Asterisks denote significance, Fisher's exact test with Benjamini-Hochberg multiple testing correction at an FDR of 0.05. **(B)** A549 IFNL1 reporter cells were infected with $NS1_{stop}$ virus at an MOI of 0.1 and either stained for HA and NS1 (HA), or M2 and NS1 (M, NS). For HA and M, cells were gated on the median NS1 staining observed in $IFNL1^+$ $NS1^+$ cells prior to measuring presence and absence of the given segment in $IFNL1^+$ and $IFNL1^-$ cells. For NS, the same was performed save for median M2 staining was used to identify infected cells. Asterisks indicate ratios significantly greater than 1 (dotted line), two-tailed one-sample t test with Benjamini-Hochberg multiple testing correction at an FDR of 0.05. Individual replicates shown, n=3. Full data with replicates shown in S11 Fig

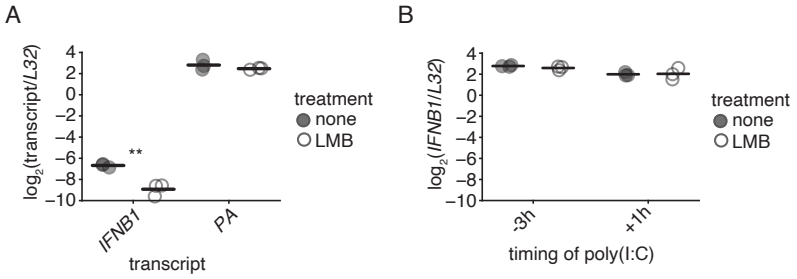

Fig 7. CRM1-dependent export contributes to innate detection of $NS1_{stop}$ without influencing detection of a viral mimetic.
(A) Our reporter cell line was infected with $NS1_{stop}$ virus at an MOI of 1.5. At 3hpi, cells were treated with 10 nM LMB. RNA was harvested at 8 hpi, and indicated transcripts analyzed by qPCR. Asterisks indicate a significant difference upon treatment, two-tailed t test with Benjamini-Hochberg multiple hypothesis correction at an FDR of 0.05, n=3. **(B)** Reporter cells were transfected with 50 ng poly(I:C) either 3 hours before (-3h) or 1 hour after (+1h) treatment with LMB. RNA was harvested 5h after LMB treatment, and *IFNB1* transcript levels assessed by qPCR. No samples were statistically different, two-tailed t test with Benjamini-Hochberg multiple hypothesis correction at an FDR of 0.05, n=3.

statistically significant, indicating that the suppression of interferon induction was unlikely to be due to an indirect impact on viral genome propagation. As LMB is a general inhibitor of CRM1, we additionally confirmed that treatment with LMB does not have a global impact on interferon expression by confirming that when applied before, or after, transfection with an artifical viral mimetic (poly(I:C:)), there is no significant impact on interferon transcription (Fig7B). We conclude from these data that CRM1-dependent export of viral replication products, likely through the action of M1 and NEP presents a significant contribution to interferon induction by a viral population lacking NS1.

Co-encoding of NS1 and NEP reduces the range of interferon induction by standing variation

The co-encoding of NS1 and NEP on the same segment, overlapping, with the former preventing interferon induction, and the latter promoting it, may limit interferon-promoting variation produced by naturally-occurring mutations as this virus grows. To investigate this hypothesis, we first explored whether mutations that impact both NS1 and NEP co-associate with interferon at a reduced rate than those anticipated to impact NS1 alone. To measure how natural diversity associates with interferon induction, we opted to generate a viral population likely to contain an enhanced rate of maladaptive diversity from a starting wild-type genotype, and observe how diversity associating with NEP and NS1 partitions with interferon production. We therefore grew two viral populations, from transfection using plasmids encoding the wild-type WSN genome onwards, in 96-well plates (each population therefore was effectively 96 independent viral rescues), which were passaged at a constant volume, effectively high MOI, across two passages, before supernatants were combined to form two biological replicate viral populations. These two populations were used to infect our reporter cell line, overexpressing viral polymerase to aid in replication despite high levels of polymerase deletions, at a particle-corrected MOI of 0.1, which was then sorted into interferon-enriched, and -depleted, populations at 13h post-infection, before RNA was

harvested and viral genomes subjected to deep-sequencing (S12 Fig,S13 Fig).

As expected of a high-MOI propagation, we find a high proportion of deletions, with, as anticipated, the greatest abundance in the three segments encoding the viral polymerase (S14 Fig). [45–49] Looking at sequence variation throughout the NS segment, much of which we would expect to be neutral or inactivating, we observe that variation in the region containing NS1 alone is significantly enriched in interferon-producing cells over variation in either NEP alone, or, critically, the region co-encoding NS1 and NEP (Fig8A and 8B). To confirm this effect isn't driven by only one, or a handful, of sites, we plotted this association at all sites across all replicates, and found the same relationship holds (Fig8C).

However, the variation we identified is incredibly close to, and at times equivalent to, the Illumina error rate, and some of this variation may not be loss-of-function. We therefore also wanted to explore a different form of variation, deletions. While rare, we did identify deletions in the NS segment (S14 Fig). Consistent with expections, deletions are generally enriched in this segment in cells producing interferon over those that were not (Fig8D). While deletions impacting NEP alone were so rare as to be stochastically sampled in our dataset, we were able to compare the relative enrichment of deletions overlapping both NS1 and NEP or NS1 alone. As in our single nucleotide variation data, deletions impacting NS1 alone are significantly more enriched in interferon-producing cells than those that impact both NEP and NS1 (Fig8E).

Taken together, these data suggest that inactivating mutations in the NS1 reading frame are, on average, less stimulatory if they occur in regions where NS1 and NEP overlap. Extending this concept to a common form of influenza failure, we were interested in how this phenomenon impacts the stochastic absence of the NS segment. Our data would suggest that the absence of the NS segment in wild-type virus would fail to be as immunostimulatory as a mutation inactivating NS1 alone. Using flow cytometry we find support for this hypothesis. As before, gating on HA-high cells, when we compare presence and absence of the NS segment through NS1 staining between wild-type and $NS1_{stop}$ virus, we find the order of interferon induction proceeds as wild-type $NS^+ << $ wild-type $NS^- \sim NS1_{stop}$ $NS^- < NS1_{stop}$ NS^+ (Fig8F). The absence of the NS segment in wild-type virus is therefore less stimulatory owing to the concurrent loss of NEP, reducing the probability of interferon induction due to segment absence alone by approximately two-fold—even when only considering infections with relatively high expression of influenza proteins.

Discussion

We have studied how variation in an influenza A virus lacking NS1, its primary interferon antagonist, associates with the induction of an interferon response. We find that enhanced detection in the absence of NS1 requires *de novo* viral replication, and the maximal response requires the presence of the M and NS segments, as well as the activity of CRM1. We additionally find that defective particles, bearing large internal deletions, both correlate, and anti-correlate, with interferon induction in the absence of NS1, depending on the experimental MOI. Lastly, we note that the most stimulatory outcomes that we identify in this study would be unikely to occur via natural variation (Fig9).

Our finding that $NS1_{stop}$ protects predominantly, perhaps solely, against *de novo* innate immune ligands is consistent with the original annotation of this protein as nonstructural, and its low abundance in mass spectromy analysis of influenza particles. [38, 50] Our work matches prior efforts that indicated that both replication and export are required with innate immune detection of this virus. [51] While conflicting reports have concluded that genome replication is unnecessary to detect

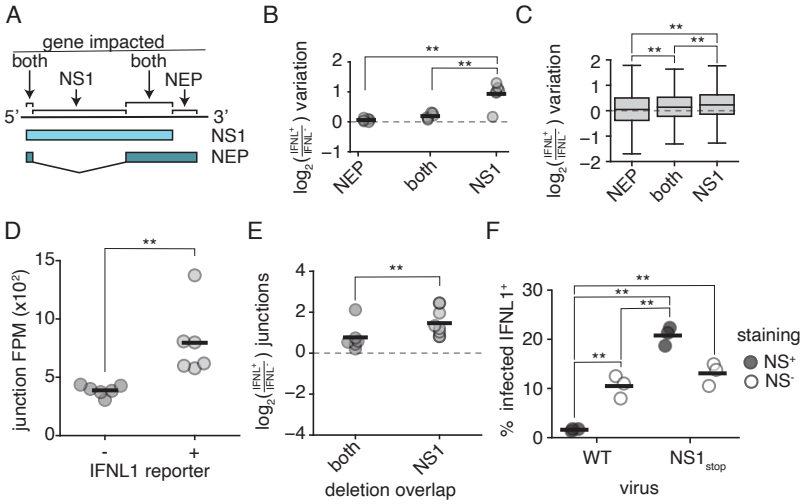

Fig 8. Co-endoding of NS1 and NEP limits the range of immune stimulation by chance mutations or segment absence$_{stop}$.
(A) Schematic of the NS segment showing the coding frames of both NS1 and NEP. Mutations that potentially impact NS1, NEP, or both, were identified in the indicated regions. **(B)** Ratio of average deviation from consensus across all sites in the regions indicated in **A**. Asterisks indicate significant difference, ANOVA $p<0.05$, post hoc Tukey's test, $q<0.05$. n=6. **(C)** Similar to **B**, but considering each site individually across all six replicates. Boxplot shows median and interquartile range. Asterisks indicate significant difference, ANOVA $p<0.05$, post hoc Tukey's test, $q<0.05$. **(D)** Normalized deletion abundance in indicated categories in the NS segment. Asterisk indicates significant difference, $p = 0.03$, n=6. **(E)** Relative, normalized, frequency of deletions in the indicated region compared between IFNL1-enriched (+) and IFNL1-depleted (-) samples. Equivalent ratio indicated by the dotted line. Significance indicated by asterisk, $p=0.01$, n=6. **(F)** The indicated viral strains were stained with HA and NS1 antibodies, and gated on the median HA value observed in IFNL1$^+$ HA$^+$ NS1$_{stop}$ infections. Presence and absence of staining for the NS1 antibody noted. Asterisks indicate significant difference, ANOVA $p<0.05$, post hoc Tukey's test, $q<0.05$, n=3. Full flow data with replicates shown in S11 Fig.

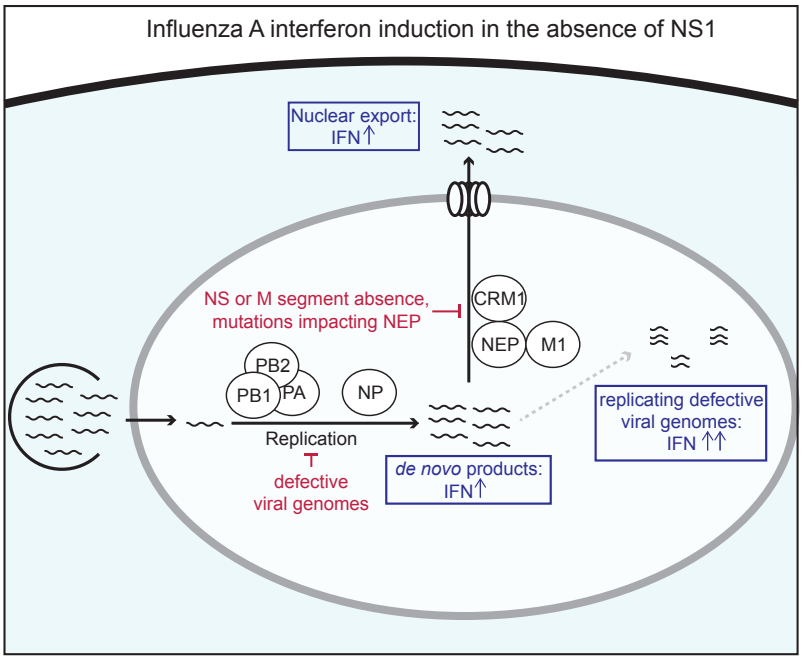

Fig 9. Conditions supporting, and suppressing, interferon induction in the absence of NS1.
Summary of major conclusions from this work. In brief, we find that both replication and export are required for maximal interferon induction in the absence of the NS1 antagonist, and that, additionally, the presence of replicating defective viral genomes greatly enhances the interferon response. Conversely, we find that the absence of the NS or M segments, mutational inactivation of NEP, or general suppression of replication, potentially through defective genome formation, all act to decrease detection of an influenza population lacking NS1. As discussed in the text, the confluence of these requirements is unlikely to occur with any great frequency in a viral population alongside the inactivation or loss of NS1.

influenza virus, and that NS1 retains relevance in that system, those efforts largely used cycloheximide, which increases interferon induction to even poly(I:C). [35, 52–54]

While we see that increasing levels of genome replication generally associate with increased interferon induction, there comes a point for a low-defective $NS1_{stop}$ population where the probability of interferon induction plateaus. This suggests that there are additional mechanisms, besides NS1 activity, that can, at least to some extent, prevent detection of *de novo* non-defective genome products. These could include occlusion of 5' triphosphate vRNA ends by the heterotrimeric polymerase, inhibition of the host response by the alternative products PA-X or PB1-F2, or interaction of PB2 directly with MAVS. [55–57] Interestingly, this limit can be overcome in the presence of defective viral genomes, as a high-defective $NS1_{stop}$ population induces interferon nearly 100% of the time in cells with high levels of viral expression. This synergistic enhancement of the interferon response indicates that NS1 acts to suppress detection of defective viral genomes.

The importance of nuclear export for interferon induction by $NS1_{stop}$ is consistent with the idea that *de novo* generated ligands are primarily detected by innate immune receptors in the cytoplasm. We do note that, while diminished, interferon induction can still occur in response to an $NS1_{stop}$ virus during leptomycin treatment, or in the absence of detectible products from the M and NS segments. This indicates that there exist ligands for RIG-I that are not exported via the canonical CRM1-M1-NEP influenza pathway. One possibility is mini viral RNAs (mvRNAs), aberrant viral replication products that contain large internal deletions, so large that they likely cannot package and can replicate in a nucleoprotein-independent fashion owing to their short length. [30] These species can trigger interferon induction in a minigenome system, which lacks both NEP and M1, and have been found in the cytoplasm, suggesting they may access this compartment through an alternate pathway to vRNPs. [31] Another possibility is nuclear-localized RIG-I, which has been suggested by several studies. [58–60] Regardless, our work provides further evidence that the cytoplasm is a critical compartment for sensing influenza virus, at least in the absence of NS1.

A theme that emerges from these observations is that, considering the common characteristics of influenza infections and the range of variation most accessible to the influenza genome, the most stimulatory potential outcomes defined in this study have a low probability of occurring. For example, although defective viral genomes can be very interferon-stimulatory in the absence of NS1, the requirement of *de novo* generated ligands for interferon induction means that most defective particles instead suppress interferon induction by $NS1_{stop}$ due to the lack of a functional viral polymerase in the absence of coinfection. If coinfection occurs, we would expect it would be highly unlikely that both infecting particles bear defects in the NS segment. In this scenario, not only would the polymerase be complemented, but any defects in NS1 would likely be suppressed. Lastly, a requirement for the activity of NEP for maximal interferon induction means that the co-encoding of NS1 and NEP effectively reduces interferon induction by variation which concurrently inactivates both proteins, either through overlapping mutations or else due to the stochastic absence of this entire segment.

By studying variation in interferon induction by the $NS1_{stop}$ virus, we were able to make inferences about what kinds of viral ligands NS1 protects and to identify viral features other than NS1 that modulate innate immune detection of influenza A virus. We find that NS1 primarily acts to prevent detection of *de novo* generated viral ligands that are exported to the cytoplasm—in the absence of NS1, interferon induction can be suppressed by low levels of viral polymerase activity or impaired nuclear export. Our study does not specifically identify what viral products act as the key RIG-I ligands in influenza infections, as *de novo* products could include full length vRNPs, defective genome segments, or mvRNAs. Further work is needed to determine the contribution of

each of these viral species to interferon induction, and whether NS1 acts equally to protect against these potential ligands. As demonstrated by our results showing a variable impact of deletions on interferon induction depending on MOI, the relative contributions of different innate immune ligands are likely context-dependent, and thus different experimental conditions may result in varying conclusions as to the importance of a given ligand. Critically, our work shows the value in considering standing variation and nonlinear impacts of events such as coinfection, and the role that such events may play in explaining the observed rarity of the interferon response to viral infection. This is important not just in our understanding of natural diversity, but also the role such variation may play in the design of artificial populations that induce a high level of interferon induction.

Materials and methods

Cell lines and viruses

The following cell lines were used in this study: HEK293T (ATCC CRL-3216), MDCK-SIAT1 (variant of the Madin Darby canine kidney cell line overexpressing SIAT1 (Sigma-Aldrich 05071502)) and A549 (human lung epithelial carcinoma cell line, ATCC CCL-185). A variant of MDCK-SIAT1 overexpressing influenza NS1 from A/PR8/1934 was generated using a lentiviral vector as previously described. [61–63] The sequence of the vector used to generate this line is provided in S4 File. A549 type I and type III interferon reporter lines were previously described. [10] A549 cells overexpressing PB1, PB2, and PA were generated using lentiviral transduction. Cell lines were tested for mycoplasma using the LookOut Mycoplasma PCR Detection Kit (Sigma-Aldrich) using JumpStart Taq DNA Polymerase (Sigma-Aldrich). A549 cells used in all sequencing experiments had their identity confirmed via STR profiling by ATCC. All cell lines were maintained in D10 media (DMEM supplemented with 10% heat-inactivated fetal bovine serum and 2 mM L-Glutamine) in a 37°C incubator with 5% CO_2. Leptomycin B (Catologue 501748123 from Fisher Scientific) was used at a final concentration of 10nM. Ribavirin (Abcam catalog ab120660) was used at a final concentration of 200μM.

A/WSN/1933 (H1N1) virus was created by reverse genetics using plasmids pHW181-PB2, pHW182-PB1, pHW183-PA, pHW184-HA, pHW185-NP, pHW186-NA, pHW187-M, pHW188-NS. [64] Genomic sequence of this virus provided in S1 File. The variant NS sequence of our $NS1_{stop}$ is also included in this file. HEK293T to MDCK-SIAT1 cells were seeded in an 8:1 coculture and transfected using BioT (Bioland Scientific, LLC) 24 hours later with equimolar reverse genetics plasmids. 24 hours post transfection, D10 media was changed to Influenza Growth Medium (IGM, Opti-MEM supplemented with 0.04% bovine serum albumin fraction V, 100 μg/ml of $CaCl_2$, and 0.01% heat-inactivated fetal bovine serum). 48 hours post-transfection for wild-type virus, and 72 hours post-transfection for $NS1_{stop}$ virus, viral supernatant was collected, centrifuged at 300g for 4 minutes to remove cellular debris, and aliquoted into cryovials to be stored at -80°C. Thawed aliquots were titered by $TCID_{50}$ on MDCK-SIAT1 cells and calculated using the Reed and Muench formula, titered by qPCR against the viral segment PA, or titered by hemagglutination. [65] To generate $NS1_{stop}$, 293T cells were co-transfected with an additional vector constituitively expressing NS1 from A/PR8/1934, and MDCK-SIAT1 cells constituitively expressing the same NS1 were used in co-culture.

To generate low-defective $NS1_{stop}$ virus, MDCK-SIAT1-NS1 cells were infected at an MOI of 0.05, and infection was allowed to proceed for 48h prior to harvest of viral supernatant, removal of debris by centrifugation, and storage in cryovials at -80°C. For low-defective wild-type virus, MDCK-SIAT1 cells were infected at an MOI of 0.05 for

36h, after which viral supernatant was harvested in an identical manner.

To genereate high-defective $NS1_{stop}$, 100μl of supernatant from our reverse genetics rescue was used to infect 500,000 MDCK-SIAT1 cells expressing NS1 in a 6-well plate. At 48h, 100μl of this supernatant was then harvested and used to infect 500,000 more MDCK-SIAT1 cells expressing NS1 in a 6-well plate. The resulting supernatant was harvested and clarified after 48h to form our high-defective $NS1_{stop}$ stock.

To generate high-defective, highly complex, wild-type virus, for each biological replicate, reverse-genetics was performed in every well of a 96-well plate. After 48h, 10μl of supernatant was transferred to fresh wells, each seeded with 10,000 MDCK-SIAT1 cells. After 48h, 10μl of that supernatant was transferred to fresh wells, each seeded with 10,000 MDCK-SIAT1 cells. After 48h, all supernatants were harvested, pooled, and clarified, to genereate one biological replicate viral population.

Single-cell transcriptomics analysis

A549 cells were infected with $NS1_{stop}$ or wild-type A/WSN/1933 at an MOI of 0.2. At 13hpi, cells were trypsonized, harvested, spun down at 300g, washed in PBS, counted using a hemocytometer, and mixed with MDCK-SIAT1 such that the latter was ∼5% of the population. This mixture was then fixed in 100% methanol for 10 minutes at -20°C. Cells were then spun down at 300g and resuspended in PBS. Cells were then counted on a hemocytometer, and loaded into the 10x Chromium instrument at a density intended to capture 2500 cells. This sample was then processed to create libraries for Illumina 3′-end sequencing according to the 10x Genomics protocol using the Chromium Single Cell 3′ Library and Gel Bead kit v2, and sequenced to a total depth of ∼80 million reads. Cell-gene matrices, and bamfiles, were generated using Cellranger version 1.3.1.

Data were then analyzed similar to Russell et al 2019 using human reads associated with canine reads to estimate background contamination rates. [10] In brief, absolute counts of transcripts of interest (interferon, influenza) were identified in canine cells, and an average contamination fraction was calculated. To correct for differences in total transcript number between canine and human cells, this fraction was modified using the relative difference in transcript number as measured in rare, co-occupied emulsions. Thereafter, to infer positivity above some threshold, contamination was assumed to be a Poisson process, sampling at a rate equivalent to this contamination frequency. Empirical q-value and p-value cutoffs were then derived from curves observed from this process. Full code and analysis provided as python scripts and jupyter notebooks at (`https://github.com/Russell-laboratory/NS1_interferon_variation`). [66]

For UMAP analysis, curated gene-cell matrices, using cell identities as defined in our custom python code, and binary infected/not-infected and interferon-positive/not-positive calls, but otherwise with no modification to gene-cell transcript counts, were used. These data were loaded into Seurat and processed according to standard protocols. [67, 68] In brief, data were normalized, variable features were identified, and data were scaled, prior to running a PCA. After running an elbow plot, neighbors were identified using 15 components from our PCA. Clusters were then identified at a resolution of 0.04. UMAP was then run with 15 components, and the resulting UMAP plot was used to graph features identified in our Python analysis. Code to re-run this analysis provided in an R-markdown file in (`https://github.com/Russell-laboratory/NS1_interferon_variation`).

For wild-type virus data, cutoffs were found to be lower for influenza positivity than our $NS1_{stop}$ dataset when derived empirically from spiked canine cells. Therefore, in order to reduce bias in our segment frequency comparisons based on this threshold, we used the higher $NS1_{stop}$ threshold rather than the empirically-determined threshold from canine cells.

Flow cytometry

Indicated cells were seeded 24 hours prior to infection, and, at the indicated time points, trypsinized and resuspended in PBS supplemented with 2% of heat-inactivated fetal bovine serum (FBS). For HA staining, cells were stained with 10 μg/ml of H17-L19, a mouse monoclonal antibody. [61] For NS1 staining, rabbit polyclonal sera, genetex catalogue GTX125990, was used at a 1:100 dilution.

For M2 staining, a mouse monoclonal antibody 14C2, from ThermoFisher Scientific was used at a concentration of 10μg/ml. Secondary antibodies were either goat anti-mouse IgG conjugated to allophycocyanin, or goat anti-mouse IgG conjugated to Alexa Fluor 405. Fixation, permeabilization and staining used BD Cytofix/Cytoperm, following manufacturers instructions.

Data processing consisted of first generating a debris gate in FlowJo prior to export to a tsv or csv and analysis using custom Python scripts, enumarated in our github repository (`https://github.com/Russell-laboratory/NS1_interferon_variation`). Uninfected controls were used to set empirical gates for influenza staining and interferon reporter positivity at a 99.9% exculsion criteria. Additional gating schema described in the text, and the accompanying code.

qPCR

Code generating graphs in manuscript can be found at `https://github.com/Russell-laboratory/NS1_interferon_variation`. Primers for all qPCR analyses listed in S5 File. RNA was purified from infected cells or viral supernatant using the Monarch total RNA miniprep kit from New England Biolabs following manufacturer's instructions. For supernatant titering, 100μl of viral supernatant was mixed with 700μl of lysis buffer for processing. cDNA from lysate for titering or qPCR was generated using the High Capacity First Strand Synthesis Kit (Applied Biosystems, 4368814) with random hexamers according to the manufacturer's protocol using a final lysate concentration of 10% of the reaction volume. qPCR was thereafter performed using Luna Universal qPCR Master Mix (New England Biolabs, M3003) with manufacturer's suggested reaction conditions.

Magnetic sorting and vRNA sequencing

For each technical replicate (3) of each biological replicate (2) high-defective wild-type virus was used to infect seven million cells apiece of three different A549 IFNL1 reporter lines, each expressing a single polymerase protein (PB1, PB2, PA). Expression was heterogeneous as these cells were bulk transduced at a high MOI. At 12h post infection, cells were trypsinized, trypsin was quenched with D10 medium, and cells were resuspended in degassed PBS supplemented with 0.5% bovine serum albumin and 5 mM EDTA. Cells were then incubated with anti-LNGFR MACSelect microbeads (Miltenyi Biotec, cataolog 130-091-330), and the pooled population was split in half and each half was loaded on an MS column (Miltenyi Biotec, catalog 130-042-201). Flow through was retained as our interferon-depleted population. To procure further enrichment of our enriched population, cells retained on each MS column were eluted by removal from a magnet, and run on a third MS column.

RNA was then harvested using QIAGEN RNeasy mini kit (QIAGEN, catalog 74104), and quantitated using a UV absorption. 1μg of RNA was converted to cDNA using universal influenza primers from Hoffmann *et al.* (2001) III and the superscript First-Strand Synthesis SuperMixkit(Invitrogen,18080400) according to the manufacturer's protocol for random-hexamer priming. [69]. qPCR was performed to

normalize the amount of influenza-specific transcripts in our cDNA pool between enriched- and depleted-samples. PCR was then performed as per Hoffmann *et al.* (2001) for 16 cycles using Q5 polymerase master mix from New England Biolabs (catalog M0492). Resulting cDNA was then tagmented using the Nextera DNA Flex LPK kit (catolog 20018704) and indexed for sequencing using Nextera compatible unique dual indices (20027213), and sequenced on a paired-end 100bp run on a Novaseq 6000 platform.

Computational analysis of deletions and single-nucleotide variation

Single-cell data used a similar pipeline as Hamele *et al.* to call deletions in individual, infected, cells. [25] Reads containing discontinuities mapping to the influenza genome were first extracted from the cellranger-generated bamfile. As these reads were mapped using the splice-aware aligner STAR, their mapping inappropriately evokes a splice-aware scoring model. Reads were remapped against the influenza genome using BLASTn, with the custom arguments of a percent identity of 90%, a word size of 10, a gap open penalty of 5, a gap extend penalty of 2, and an e-value cutoff of 0.000001. A custom script was then used to annotate deletions identified in the BLAST file. No set number of bases are required on either side, however a single BLAST mapping is required, with all bases in the read assigned to a mapping. When bases repeat on both sides of the junction, they are arbitrarily assigned to the 5' end as defined in the polarity of our FASTA file. Reads mapping to known splice sites in the M and NS segments were removed from further analysis. Lastly, read names were compared to the original bamfile and assigned cell barcodes.

Thereafter, to reduce our calls to a set of confidently-mapped deletions, the total number of emulsions associated with a given deletion was calculated. Deletions that are perhaps simply lysis-associated, or associated with some common template-switching event, would likely be dispersed across many emulsions, whereas true, biologically-relevant, deletions would likely be associated with only a subset of emulsions. A cutoff was then empirically derived where this curve was observed to flatten, in an attempt to both maximize sensitivity and accuracy of our calls. This ended up being a cutoff of read support at 20nt. To determine the frequency of likely full-length co-occurrence with deletions, reads without a gap adjacent to the observed junction were enumerated with a custom script. Reads above our segment absence threshold were considered to support the existence of full-length segments alongside deletions.

For bulk-sequencing, deletion-calling used the pipeline described in Mendes *et al.*. [35] Reads were processed by Trimmomatic, providing Nextera adapter sequeces and the following variables: 2 seed mismatches, a palindrome clip threshold of 30, a simple clip threshold of 10, a minimum adapter length of 2, keep both reads, a lead of 20, a sliding window from 4 to 15, and a minimum retained length of 36. [70] Read1 and 2 were mapped independently against the A/WSN/1933 genome ng STAR, with a requirement to map without gaps. Large regions of mismatches were excluded, as were large deletions. Unmapped reads were retained, and used in a BLASTn search as described above for single-cell data. BLAST output was parsed as above, and deletions present in all technical replicates retained for a custom GTF. This custom GTF was used to remap unmapped reads using STAR, and deletions were enumerated on a per/fragment basis using a custom script and samtools. [71] For the NS segment, specifically, owing to the rarity of deletions, thresholds were dropped and BLAST mapping was used to call deletions in addition to using our custom GTF.

For nucleotide variation, we used the same final bamfiles as described above with our multiple rounds of mapping. We considered all sites with a quality score greater than 30.

We then measured all non-concensus variation, regardless of its threshold. As we were comparing between two conditions, we did not consider normal minor-variant thresholding, with the understanding that the error rate of reverse-transcription and sequencing should be relatively well controlled between sample sets, and, even moreso, when comparing different regions in the same segment.

0.1 Data availability

Sequencing data are availalble at GSE215914. Code for analysis available at `https://github.com/Russell-laboratory/NS1_interferon_variation`.

Supporting information

S1 File. Sequence of wild-type and $NS1_{stop}$ viruses.

S2 File. All deletion junctions and number of supporting reads from single-cell sequencing

S3 File. All deletion junctions and number of supporting reads from bulk sequencing

S4 File. Sequence of construct used to generate NS1-expressing MDCK-SIAT1 cells

S5 File. Sequences of all qPCR primers used in this study

S1 Fig. Data supporting thresholds used in Fig1 Thresholding for human cells based on contaminating fractions in canine cells for $NS1_{stop}$. **(A)** Distribution of human transcripts found in cells identified as canine by Cellranger software. We found misannotation of some doublets, which we reannotated, denoted by the dotted line, **(B)** Distribution of canine transcripts found in cells identified as human by Cellranger. No signs of misannotation as in **A**. **(C)** Final droplet annotations after modification. **(D)** Distribution of transcript counts in droplets annotated as containing only human cells. To try and exclude doublets from further analysis, droplets with content greater than the dotted line were excluded. **(E)** Using inferred contamination from **A** and **C**, assuming a constant fraction of reads contaminating droplets, with a correction for the relative number of transcripts recovered from human versus canine droplets, q values were interpolated from p-values assuming a Poisson sampling and Benjamini-Hochberg multiple testing correction. Empirically-derived thresholds were derived, as shown by the dotted line, at inflection points for interferons and at a reasonably conservative estimate for influenza. Data show the cumulative density function (cdf), the fraction of droplets (of the total) that meet the indicated threshold.

S2 Fig. Data supporting thresholds used in Fig1 Thresholding for human cells based on contaminating fractions in canine cells for wild-type virus. **(A)** Distribution of human transcripts found in cells identified as canine by Cellranger software. We found misannotation of some doublets, which we reannotated, denoted by the dotted line, **(B)** Distribution of canine transcripts found in cells identified as human by Cellranger. No signs of misannotation as in **A**. **(C)** Final droplet annotations after modification. **(D)** Distribution of transcript counts in droplets annotated as containing only human cells. To try and exclude doublets from further analysis, droplets with content greater than

the dotted line were excluded. **(E)** To maintain comparability between datasets, thresholds were used from $NS1_{stop}$ data. The indicated numbers were procured from this threshold. **(F)** Distribution of the fraction of reads derived from influenza in infected cells.

S3 Fig. Full flow data for Fig2 and Fig3 Data showing full flow data and measurements of IFNL1 reporter, and HA staining. Cells infected at an MOI of 0.1, measurements made 13h post-infection. Individual replicates shown. Interferon-positive events colored in orange. Data subsetted to 5000 events to show equivalent numbers between conditions.

S4 Fig. Probability of interferon production relates to HA staining The fraction of cells expressing IFNL1 reporter in each bin of HA expression from experiment represented in Fig2B and 3B. R value, Spearman correlation. n=4. Individual replicates shown.

S5 Fig. Ribavirin suppresses influenza replication Measurement of *HA* transcripts from experiment shown in Fig3C. Asterisk indicates significant difference, two-tailed t test, $p=10^{-3.8}$.

S6 Fig. Thresholds for calling deletions in Fig4A The number of average emulsions associated with any given deletion at the indicated read support is shown. At lower read support, deletions are more broadly distributed, suggesting contamination or template-switching. At higher support, they are less broadly distributed, suggesting bone-fide deletions. Cutoff chosen for this study indicated by the dotted line.

S7 Fig. Full flow data for Fig5 Data showing full flow data and measurements of IFNL1 reporter, and M2 staining. Cells infected the indicated, particle-corrected MOI, and measurements made 13h post-infection. Individual replicates shown. Interferon-positive events colored in orange. Data subsetted to 5000 events to show equivalent numbers between conditions.

S8 Fig. Full distributions of M2 staining for Fig5C,D Density distributions for M2 staining from S7 Fig

S9 Fig. Thresholds for segment presence in Fig6 The fraction of influenza positive cells that meet the indicated p-value threshold for presence of the indicated segment from our calculations using contamination measured by canine cells. P-values rather than q-values were used as both presence and absence are of interest, and we have pre-conditioned on influenza-positive cells alone. Dotted lines indicate p-value thresholds for positivity.

S10 Fig. anti-NS1 antibody retains staining even with truncated $NS1_{stop}$ Staining profile of 293T cells transfected with plasmids expressing the four influenza polymerase components (PB2, PB1, PA, and NP) and a plasmid encoding the indicated vRNA. HA-mCherry served as a negative control.

S11 Fig. Full flow data for Fig6B and Fig8F (A) Data showing full flow data and measurements of IFNL1 reporter, M2, and NS1 staining of $NS1_{stop}$ variant. Cells infected at an MOI of 0.1, measurements made 13h post-infection. Individual replicates shown. Interferon-positive events colored in orange. Data subsetted to 5000 events to

show equivalent numbers between conditions. **(B)** Same as in **A**, save for wild-type virus was also used and staining was for HA and NS1.

S12 Fig. Flow data justifying use of complementing cell lines in Fig8B-E Both high-defective wild-type populations were used to infect IFNL1 reporter cells at an MOI of 0.1, and stained for HA at 13h post infection. IFNL1 reporter cells were complemented, individually, with each of the three polymerase segments. An increase in HA staining was observed in each condition, as well as an increase in the fraction of responding cells.

S13 Fig. qPCR validation of IFNL1 sorting used for Fig8B-E qPCR against HA (top) or IFNβ (bottom) normalized to the housekeeping control L32 of triplicate technical replicate, biological duplicate, high-defective wild-type populations infecting IFNL1 reporter cells, sorted on IFNL1 reporter expression. As expected, both infection and interferon expression was enriched during our sort. Each point indicates a technical replicate measurement of transcript values for each individual experimental technical replicate and biological replicate.

S14 Fig. Deletion abundance in RNAseq data presented in Fig8B-E Using the pipeline described in methods, both total fragments, and unique fragments, mapped to deletions in each segment across all six replicate experiments. The NS segment was assessed using lower thresholds, as described in methods, to pick up rare, stochastic, events in this segment.

Acknowledgments

Reserach reported in this publication was supported by the National Institute of General Medical Sciences of the National Institutes of Health under award number R35GM147031. ACV was supported by a National Instutites of Health T32 grant award number T32GM133351.

References

1. Iwasaki A, Pillai PS. Innate immunity to influenza virus infection. Nature Reviews Immunology. 2014;14(5):315–328. doi:10.1038/nri3665.

2. McNab F, Mayer-Barber K, Sher A, Wack A, O'Garra A. Type I interferons in infectious disease. Nature Reviews Immunology. 2015;15(2):87–103. doi:10.1038/nri3787.

3. Randall RE, Goodbourn S. Interferons and viruses: an interplay between induction, signalling, antiviral responses and virus countermeasures. Journal of General Virology. 2008;89(1):1–47. doi:10.1099/vir.0.83391-0.

4. Dimmock NJ, Easton AJ. Defective Interfering Influenza Virus RNAs: Time To Reevaluate Their Clinical Potential as Broad-Spectrum Antivirals? Journal of Virology. 2014;88(10):5217–5227. doi:10.1128/jvi.03193-13.

5. García-Sastre A. Ten Strategies of Interferon Evasion by Viruses. Cell Host & Microbe. 2017;22(2):176–184. doi:10.1016/j.chom.2017.07.012.

6. Opitz B, Rejaibi A, Dauber B, Eckhard J, Vinzing M, Schmeck B, et al. IFNB induction by influenza A virus is mediated by RIG-I which is regulated by the viral NS1 protein. Cellular Microbiology. 2007;9(4):930–938. doi:10.1111/j.1462-5822.2006.00841.x.

7. García-Sastre A, Egorov A, Matassov D, Brandt S, Levy DE, Durbin JE, et al. Influenza A Virus Lacking the NS1 Gene Replicates in Interferon-Deficient Systems. Virology. 1998;252(2):324–330. doi:10.1006/viro.1998.9508.

8. Killip MJ, Jackson D, Pérez-Cidoncha M, Fodor E, Randall RE. Single-cell studies of IFN-B promoter activation by wild-type and NS1-defective influenza A viruses. Journal of General Virology. 2017;98(3):357–363. doi:10.1099/jgv.0.000687.

9. Chen S, Short JAL, Young DF, Killip MJ, Schneider M, Goodbourn S, et al. Heterocellular induction of interferon by negative-sense RNA viruses. Virology. 2010;407(2):247–255. doi:10.1016/j.virol.2010.08.008.

10. Russell AB, Elshina E, Kowalsky JR, Velthuis AJWT, Bloom JD. Single-Cell Virus Sequencing of Influenza Infections That Trigger Innate Immunity. Journal of virology. 2019;93(14). doi:10.1128/jvi.00500-19.

11. Donald HB, Isaacs A. Counts of Influenza Virus Particles. Journal of General Microbiology. 1954;10(3):457–464. doi:10.1099/00221287-10-3-457.

12. Brooke CB, Ince WL, Wrammert J, Ahmed R, Wilson PC, Bennink JR, et al. Most Influenza A Virions Fail To Express at Least One Essential Viral Protein. Journal of Virology. 2013;87(6):3155–3162. doi:10.1128/jvi.02284-12.

13. Russell AB, Trapnell C, Bloom JD. Extreme heterogeneity of influenza virus infection in single cells. eLife. 2018;7. doi:10.7554/elife.32303.

14. Meyts I, Casanova J. Viral infections in humans and mice with genetic deficiencies of the type I IFN response pathway. European Journal of Immunology. 2021;doi:10.1002/eji.202048793.

15. Ciancanelli MJ, Huang SXL, Luthra P, Garner H, Itan Y, Volpi S, et al. Life-threatening influenza and impaired interferon amplification in human IRF7 deficiency. Science. 2015;348(6233):448–453. doi:10.1126/science.aaa1578.

16. Haller O, Arnheiter H, Lindenmann J, Gresser I. Host gene influences sensitivity to interferon action selectively for influenza virus. Nature. 1980;283(5748):660–662. doi:10.1038/283660a0.

17. Robb NC, Smith M, Vreede FT, Fodor E. NS2/NEP protein regulates transcription and replication of the influenza virus RNA genome. Journal of General Virology. 2009;90(6):1398–1407. doi:10.1099/vir.0.009639-0.

18. Chua M, Schmid S, Perez J, Langlois R, tenOever B. Influenza A Virus Utilizes Suboptimal Splicing to Coordinate the Timing of Infection. Cell Reports. 2013;3(1):23–29. doi:10.1016/j.celrep.2012.12.010.

19. O'Neill RE, Talon J, Palese P. The influenza virus NEP (NS2 protein) mediates the nuclear export of viral ribonucleoproteins. The EMBO Journal. 1998;17(1):288–296. doi:10.1093/emboj/17.1.288.

20. Paterson D, Fodor E. Emerging Roles for the Influenza A Virus Nuclear Export Protein (NEP). PLoS Pathogens. 2012;8(12):e1003019. doi:10.1371/journal.ppat.1003019.

21. Zilionis R, Nainys J, Veres A, Savova V, Zemmour D, Klein AM, et al. Single-cell barcoding and sequencing using droplet microfluidics. Nature Protocols. 2017;12(1):44–73. doi:10.1038/nprot.2016.154.

22. Klein A, Mazutis L, Akartuna I, Tallapragada N, Veres A, Li V, et al. Droplet Barcoding for Single-Cell Transcriptomics Applied to Embryonic Stem Cells. Cell. 2015;161(5):1187–1201. doi:10.1016/j.cell.2015.04.044.

23. Hay AJ, Lomniczi B, Bellamy AR, Skehel JJ. Transcription of the influenza virus genome. Virology. 1977;83(2):337–355. doi:10.1016/0042-6822(77)90179-9.

24. Plotch SJ, Bouloy M, Ulmanen I, Krug RM. A unique cap(m7GpppXm)-dependent influenza virion endonuclease cleaves capped RNAs to generate the primers that initiate viral RNA transcription. Cell. 1981;23(3):847–858. doi:10.1016/0092-8674(81)90449-9.

25. Hamele CE, Russell AB, Heaton NS. In Vivo Profiling of Individual Multiciliated Cells during Acute Influenza A Virus Infection. Journal of Virology. 2022;96(14):e00505–22. doi:10.1128/jvi.00505-22.

26. Sun J, Vera JC, Drnevich J, Lin YT, Ke R, Brooke CB. Single cell heterogeneity in influenza A virus gene expression shapes the innate antiviral response to infection. PLOS Pathogens. 2020;16(7):e1008671. doi:10.1371/journal.ppat.1008671.

27. Wang C, Forst CV, Chou TW, Geber A, Wang M, Hamou W, et al. Cell-to-Cell Variation in Defective Virus Expression and Effects on Host Responses during Influenza Virus Infection. mBio. 2020;11(1). doi:10.1128/mbio.02880-19.

28. Ramos I, Smith G, Ruf-zamojski F, Martinez-Romero C, Fribourg M, Carbajal EA, et al. Innate immune response to influenza virus at single-cell resolution in human epithelial cells revealed paracrine induction of interferon lambda 1. Journal of Virology. 2019;doi:10.1128/JVI.00559-19.

29. Rehwinkel J, Tan CP, Goubau D, Schulz O, Pichlmair A, Bier K, et al. RIG-I detects viral genomic RNA during negative-strand RNA virus infection. Cell. 2010;140(3):397–408. doi:10.1016/j.cell.2010.01.020.

30. Velthuis AJt, Long JC, Bauer DL, Fan RL, Yen HL, Sharps J, et al. Mini viral RNAs act as innate immune agonists during influenza virus infection. Nature Microbiology. 2018;3(11):1234–1242. doi:10.1038/s41564-018-0240-5.

31. French H, Pitré E, Oade MS, Elshina E, Bisht K, King A, et al. Transient RNA structures cause aberrant influenza virus replication and innate immune activation. Science Advances. 2022;8(36):eabp8655. doi:10.1126/sciadv.abp8655.

32. Baum A, Sachidanandam R, García-Sastre A. Preference of RIG-I for short viral RNA molecules in infected cells revealed by next-generation sequencing. Proceedings of the National Academy of Sciences. 2010;107(37):16303–16308. doi:10.1073/pnas.1005077107.

33. Bean WJ, Simpson RW. Primary transcription of the influenza virus genome in permissive cells. Virology. 1973;56(2):646–651. doi:10.1016/0042-6822(73)90067-6.

34. Velthuis AJWt, Fodor E. Influenza virus RNA polymerase: insights into the mechanisms of viral RNA synthesis. Nature Reviews Microbiology. 2016;14(8):479–493. doi:10.1038/nrmicro.2016.87.

35. Mendes M, Russell AB. Library-based analysis reveals segment and length dependent characteristics of defective influenza genomes. PLoS pathogens. 2021;17(12):e1010125. doi:10.1371/journal.ppat.1010125.

36. Scholtissek C. Inhibition of influenza RNA synthesis by virazole (ribavirin). Archives of Virology. 1976;50(4):349–352. doi:10.1007/bf01317961.

37. Vanderlinden E, Vrancken B, Houdt JV, Rajwanshi VK, Gillemot S, Andrei G, et al. Distinct Effects of T-705 (Favipiravir) and Ribavirin on Influenza Virus Replication and Viral RNA Synthesis. Antimicrobial Agents and Chemotherapy. 2016;60(11):6679–6691. doi:10.1128/aac.01156-16.

38. Hutchinson EC, Charles PD, Hester SS, Thomas B, Trudgian D, Martínez-Alonso M, et al. Conserved and host-specific features of influenza virion architecture. Nature Communications. 2014;5(1):4816. doi:10.1038/ncomms5816.

39. Tapia K, Kim Wk, Sun Y, Mercado-López X, Dunay E, Wise M, et al. Defective Viral Genomes Arising In Vivo Provide Critical Danger Signals for the Triggering of Lung Antiviral Immunity. PLoS Pathogens. 2013;9(10):e1003703. doi:10.1371/journal.ppat.1003703.

40. Xue J, Chambers BS, Hensley SE, López CB. Propagation and Characterization of Influenza Virus Stocks That Lack High Levels of Defective Viral Genomes and Hemagglutinin Mutations. Frontiers in Microbiology. 2016;7:326. doi:10.3389/fmicb.2016.00326.

41. Bui M, Wills EG, Helenius A, Whittaker GR. Role of the Influenza Virus M1 Protein in Nuclear Export of Viral Ribonucleoproteins. Journal of Virology. 2000;74(4):1781–1786. doi:10.1128/jvi.74.4.1781-1786.2000.

42. Martin K, Heleniust A. Nuclear transport of influenza virus ribonucleoproteins: The viral matrix protein (M1) promotes export and inhibits import. Cell. 1991;67(1):117–130. doi:10.1016/0092-8674(91)90576-k.

43. Ma K, Roy AMM, Whittaker GR. Nuclear Export of Influenza Virus Ribonucleoproteins: Identification of an Export Intermediate at the Nuclear Periphery. Virology. 2001;282(2):215–220. doi:10.1006/viro.2001.0833.

44. Kudo N, Wolff B, Sekimoto T, Schreiner EP, Yoneda Y, Yanagida M, et al. Leptomycin B Inhibition of Signal-Mediated Nuclear Export by Direct Binding to CRM1. Experimental Cell Research. 1998;242(2):540–547. doi:10.1006/excr.1998.4136.

45. Donald HB, Isaacs A. Counts of Influenza Virus Particles. Journal of General Microbiology. 1954;10(3):457–464. doi:10.1099/00221287-10-3-457.

46. Nakajima K, Ueda M, Sugiura A. Origin of small RNA in von Magnus particles of influenza virus. Journal of Virology. 1979;29(3):1142–1148. doi:10.1128/jvi.29.3.1142-1148.1979.

47. Akkina RK, Chambers TM, Nayak DP. Mechanism of interference by defective-interfering particles of influenza virus: Differential reduction of intracellular synthesis of specific polymerase proteins. Virus Research. 1984;1(8):687–702. doi:10.1016/0168-1702(84)90059-5.

48. Alnaji FG, Holmes JR, Rendon G, Vera CJ, Fields CJ, Martin BE, et al. Sequencing Framework for the Sensitive Detection and Precise Mapping of Defective Interfering Particle-Associated Deletions across Influenza A and B Viruses. Journal of Virology. 2019;93(11). doi:10.1128/jvi.00354-19.

49. Pelz L, Rüdiger D, Dogra T, Alnaji FG, Genzel Y, Brooke CB, et al. Semi-continuous propagation of influenza A virus and its defective interfering particles: analyzing the dynamic competition to select candidates for antiviral therapy. Journal of Virology. 2021; p. JVI0117421. doi:10.1128/jvi.01174-21.

50. Inglis SC, Carroll AR, Lamb RA, Mahy BWJ. Polypeptides specified by the influenza virus genome I. Evidence for eight distinct gene products specified by fowl plague virus. Virology. 1976;74(2):489–503. doi:10.1016/0042-6822(76)90355-x.

51. Killip MJ, Smith M, Jackson D, Randall RE. Activation of the Interferon Induction Cascade by Influenza A Viruses Requires Viral RNA Synthesis and Nuclear Export. Journal of Virology. 2014;88(8):3942–3952. doi:10.1128/jvi.03109-13.

52. Tan YH, Armstrong JA, Ke YH, Ho M. Regulation of Cellular Interferon Production: Enhancement by Antimetabolites. Proceedings of the National Academy of Sciences. 1970;67(1):464–471. doi:10.1073/pnas.67.1.464.

53. Raj NB, Pitha PM. Two levels of regulation of beta-interferon gene expression in human cells. Proceedings of the National Academy of Sciences. 1983;80(13):3923–3927. doi:10.1073/pnas.80.13.3923.

54. Ringold GM, Dieckmann B, Vannice JL, Trahey M, McCormick F. Inhibition of protein synthesis stimulates the transcription of human beta-interferon genes in Chinese hamster ovary cells. Proceedings of the National Academy of Sciences. 1984;81(13):3964–3968. doi:10.1073/pnas.81.13.3964.

55. Varga ZT, Ramos I, Hai R, Schmolke M, García-Sastre A, Fernandez-Sesma A, et al. The Influenza Virus Protein PB1-F2 Inhibits the Induction of Type I Interferon at the Level of the MAVS Adaptor Protein. PLoS Pathogens. 2011;7(6):e1002067. doi:10.1371/journal.ppat.1002067.

56. Graef KM, Vreede FT, Lau YF, McCall AW, Carr SM, Subbarao K, et al. The PB2 Subunit of the Influenza Virus RNA Polymerase Affects Virulence by Interacting with the Mitochondrial Antiviral Signaling Protein and Inhibiting Expression of Beta Interferon. Journal of Virology. 2010;84(17):8433–8445. doi:10.1128/jvi.00879-10.

57. Jagger BW, Wise HM, Kash JC, Walters KA, Wills NM, Xiao YL, et al. An Overlapping Protein-Coding Region in Influenza A Virus Segment 3 Modulates the Host Response. Science. 2012;337(6091):199–204. doi:10.1126/science.1222213.

58. Liu G, Lu Y, Raman SNT, Xu F, Wu Q, Li Z, et al. Nuclear-resident RIG-I senses viral replication inducing antiviral immunity. Nature Communications. 2018;9(1):3199. doi:10.1038/s41467-018-05745-w.

59. Liu G, Lu Y, Liu Q, Zhou Y. Inhibition of Ongoing Influenza A Virus Replication Reveals Different Mechanisms of RIG-I Activation. Journal of Virology. 2019;93(6). doi:10.1128/JVI.02066-18.

60. Wang C, Zhou W, Liu Y, Xu Y, Zhang X, Jiang C, et al. Nuclear translocation of RIG-I promotes cellular apoptosis. Journal of Autoimmunity. 2022;130:102840. doi:10.1016/j.jaut.2022.102840.

61. Doud MB, Bloom JD. Accurate Measurement of the Effects of All Amino-Acid Mutations on Influenza Hemagglutinin. Viruses. 2016;8(6):155. doi:10.3390/v8060155.

62. Bloom JD, Gong LI, Baltimore D. Permissive Secondary Mutations Enable the Evolution of Influenza Oseltamivir Resistance. Science. 2010;328(5983):1272–1275. doi:10.1126/science.1187816.

63. O'Connell RM, Balazs AB, Rao DS, Kivork C, Yang L, Baltimore D. Lentiviral Vector Delivery of Human Interleukin-7 (hIL-7) to Human Immune System (HIS) Mice Expands T Lymphocyte Populations. PLoS ONE. 2010;5(8):e12009. doi:10.1371/journal.pone.0012009.

64. Hoffmann E, Neumann G, Kawaoka Y, Hobom G, Webster RG. A DNA transfection system for generation of influenza A virus from eight plasmids. Proceedings of the National Academy of Sciences. 2000;97(11):6108–6113. doi:10.1073/pnas.100133697.

65. Reed LJ, Muench H. A SIMPLE METHOD OF ESTIMATING FIFTY PER CENT ENDPOINTS. American Journal of Epidemiology. 1938;27(3):493–497. doi:10.1093/oxfordjournals.aje.a118408.

66. Kluyver T, Ragan-Kelley B, Pérez F, Granger B, Bussonnier M, Frederic J, et al. Jupyter Notebooks – a publishing format for reproducible computational workflows . Positioning and Power in Academic Publishing: Players, Agents and Agendas. 2016; p. 87–90. doi:10.3233/978-1-61499-649-1-87.

67. Hao Y, Hao S, Andersen-Nissen E, III WMM, Zheng S, Butler A, et al. Integrated analysis of multimodal single-cell data. Cell. 2021;doi:10.1016/j.cell.2021.04.048.

68. McInnes L, Healy J, Saul N, Großberger L. UMAP: Uniform Manifold Approximation and Projection. Journal of Open Source Software. 2018;3(29):861. doi:10.21105/joss.00861.

69. Hoffmann E, Stech J, Guan Y, Webster RG, Perez DR. Universal primer set for the full-length amplification of all influenza A viruses. Archives of Virology. 2001;146(12):2275–2289. doi:10.1007/s007050170002.

70. Bolger AM, Lohse M, Usadel B. Trimmomatic: a flexible trimmer for Illumina sequence data. Bioinformatics. 2014;30(15):2114–2120. doi:10.1093/bioinformatics/btu170.

71. Li H, Handsaker B, Wysoker A, Fennell T, Ruan J, Homer N, et al. The Sequence Alignment/Map format and SAMtools. Bioinformatics. 2009;25(16):2078–2079. doi:10.1093/bioinformatics/btp352.